We sincerely thank the Huw Horgan referee for their very helpful comments and for thoroughly reviewing the manuscript. The comments were very valuable and helpful in improving the clarity and quality of the manuscript. We have included all the comments and responded to them in detail below. Line numbers refer to the revised manuscript version.

Comments from Huw Horgan (RC1)

Specific comments:

The manuscript would benefit from the following:
1. Some additional justification of the survey location. Figure 3 shows that the survey location falls almost entirely outside of the active lake boundary from Smith et al., 2009. Please explain why this is the case. A useful addition to Figure 3 would be to show contours of equal hydropotential. This would further support the site selection, especially if they showed a hydropotential sink (closed contours of hydropotential.)

➔ We appreciate the reviewer's valuable comment regarding the clarification of site selection for the seismic survey. In response, we have added a reference to Ju et al. (2025), which provides a detailed description of the subglacial lake boundaries inferred from ice-penetrating radar (IPR) surveys. The location of the seismic survey lines in this study was carefully determined based on the lake extent proposed by Ju et al. (2025). To improve clarity, we have revised the manuscript to explicitly state that the seismic survey was conducted within the area where the presence of a subglacial lake was inferred from radar observations. Additionally, we updated Figure 3 to include the subglacial lake extent defined by Ju et al. (2025), along with a hydraulic head map, to provide more comprehensive spatial context for the survey design.

(Page 3, Lines 71-74) "Building upon these observations, Ju et al. (2025) subdivided the previously identified single subglacial water body at SLD2, as detected by ICESat altimetry, into three smaller subglacial lakes: SLD2-A, SLD2-B, and SLD2-C. Among these, SLD2-A represents the largest areal extent, and targeted seismic surveys were conducted over this area to obtain high-resolution information on the lake depth and basal structure."

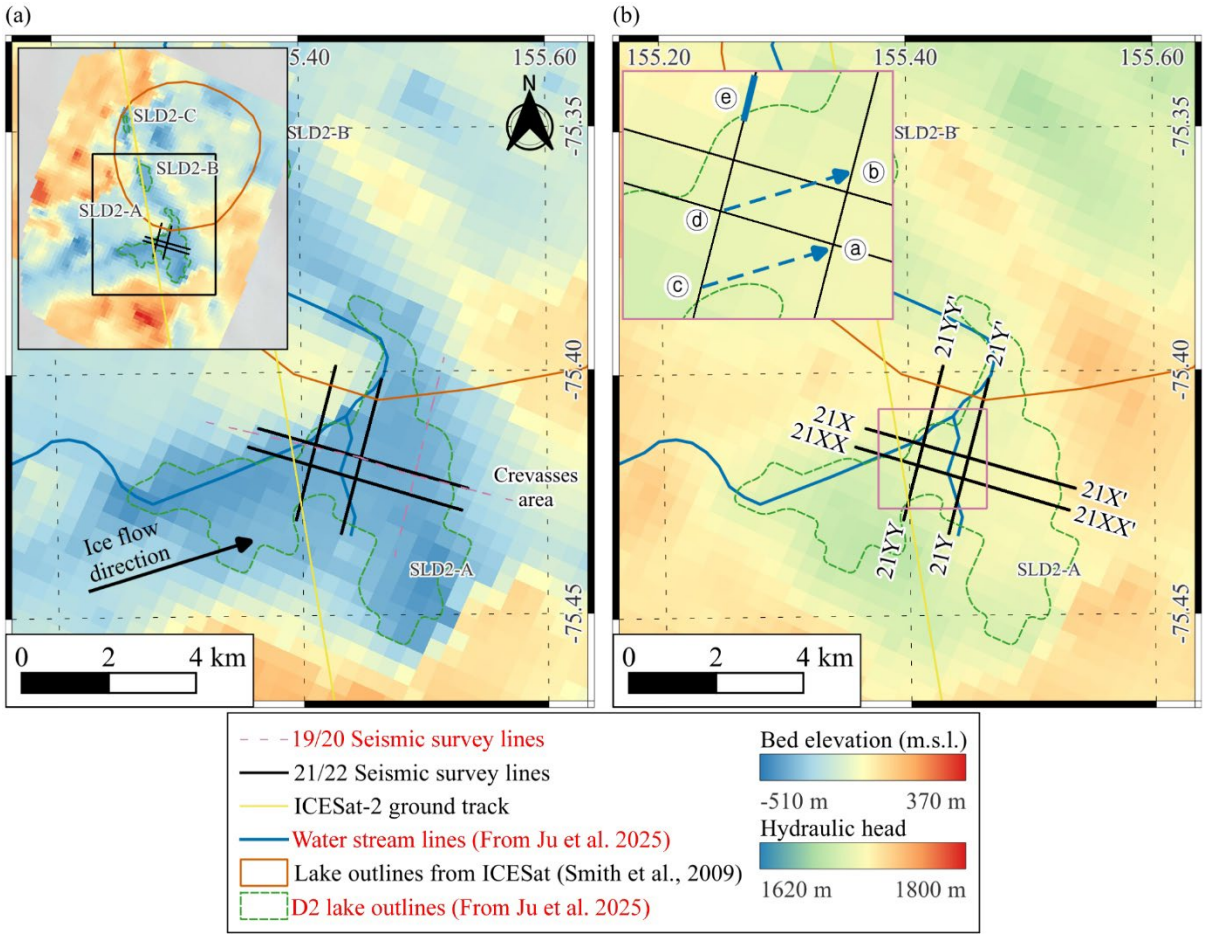

Figure 3: 21/22 seismic survey layout (black lines) overlaid on (a) bed elevation and (b) hydraulic head data from IPR results (Ju et al., 2025).

2. Please include a more detailed description of the reasons for the unsuitability of the seismic data acquired previously. This would be of benefit to other researchers as it would allow them to avoid similar pitfalls.

➔ We have revised the manuscript to include a more detailed explanation of the technical issues and limitations encountered during the preliminary seismic campaign.

(Pages 5-6, Lines 125-137) "During the 2019/20 austral summer, a preliminary seismic survey was conducted over the SLD2-A region to evaluate the potential presence of a subglacial lake and to obtain initial information on its structural characteristics. Owing to limited field time and equipment constraints, the fold of coverage for all survey lines was restricted to 1, and all shot points were aligned near surface crevasses. Consequently, the acquired seismic data were significantly contaminated by strong linear coherent noise associated with crevasses, which severely degraded the signal quality of key reflectors, particularly reflections from the subglacial lake–bedrock interface. In addition, explosives are deployed within shallow boreholes (< 20 m depth), and owing to the absence of proper backfilling and the rapid timing of detonation, poor coupling between the explosives and the borehole walls further reduces energy transmission efficiency, resulting in overall low-quality reflection signals (Ju et al., 2024). As a result, due to the limitations of single-fold acquisition, stacking was not feasible, resulting in a low signal-to-noise ratio (SNR) and the presence of dominant coherent noise, rendering the seismic dataset unsuitable for quantitative structural interpretation. Nevertheless, the preliminary survey qualitatively confirmed the glacier thickness beneath SLD2-A and suggested the presence of subglacial water, providing critical baseline information that guided the methodology and survey design of the subsequent detailed seismic campaign conducted during the 2021/22 season."

3. Seismic data can be very hard to present. I think presentation could be improved here. Reflections from and ice over water interface are high amplitude and negative polarity. The follow issues occur to me:

3.1 Figure 4. The image and zoom sections are too small for me to identify the dominant polarity in the basal returns. I suggest presenting exemplar shot records of ice over water and ice over rock, and including larger insets showing the basal returns.

➔ We have revised Figure 4 to improve the clarity of basal reflection polarity. Specifically, we have included example shot gathers for ice over water and ice over bedrock scenarios, each accompanied by enlarged inset panels that highlight the key reflection events and their respective polarities. Additionally, we have added an inset showing the direct and refracted wave velocities within the 0–0.2 s two-way travel time (TWT) range. This inset also includes an annotation of the direct wave signal to confirm the polarity of the source wavelet. These revisions provide a more comprehensive illustration of the reflection characteristics and improve interpretation accuracy.

(Page 8, Lines 160-169) “Figure 4 presents shot gather #27 from line 21X and shot gather #7 from line 21Y. In these shot gathers, the velocity of the direct wave is estimated to be approximately 1800 m/s, and the refracted wave velocity is approximately 3800 m/s. First-arrival analysis of the direct wave indicates a normal polarity, confirming the source waveform polarity. A prominent negative polarity reflection is observed at a two-way travel time (TWT) of approximately 1.2 s, interpreted as the glacier–lake interface. Approximately 25–30 ms later, a ghost reflection with normal polarity appears. A subsequent reflection at approximately 1.3 s TWT, showing normal polarity, is attributed to the lake–bed interface, followed by its negative polarity ghost reflection 25–30 ms later. In shot gather #27, noise originating from crevasses becomes apparent from approximately 2 s TWT. As the distance to the crevasses decreases, this noise increasingly overlaps with the primary reflection arrivals, complicating the interpretation.”

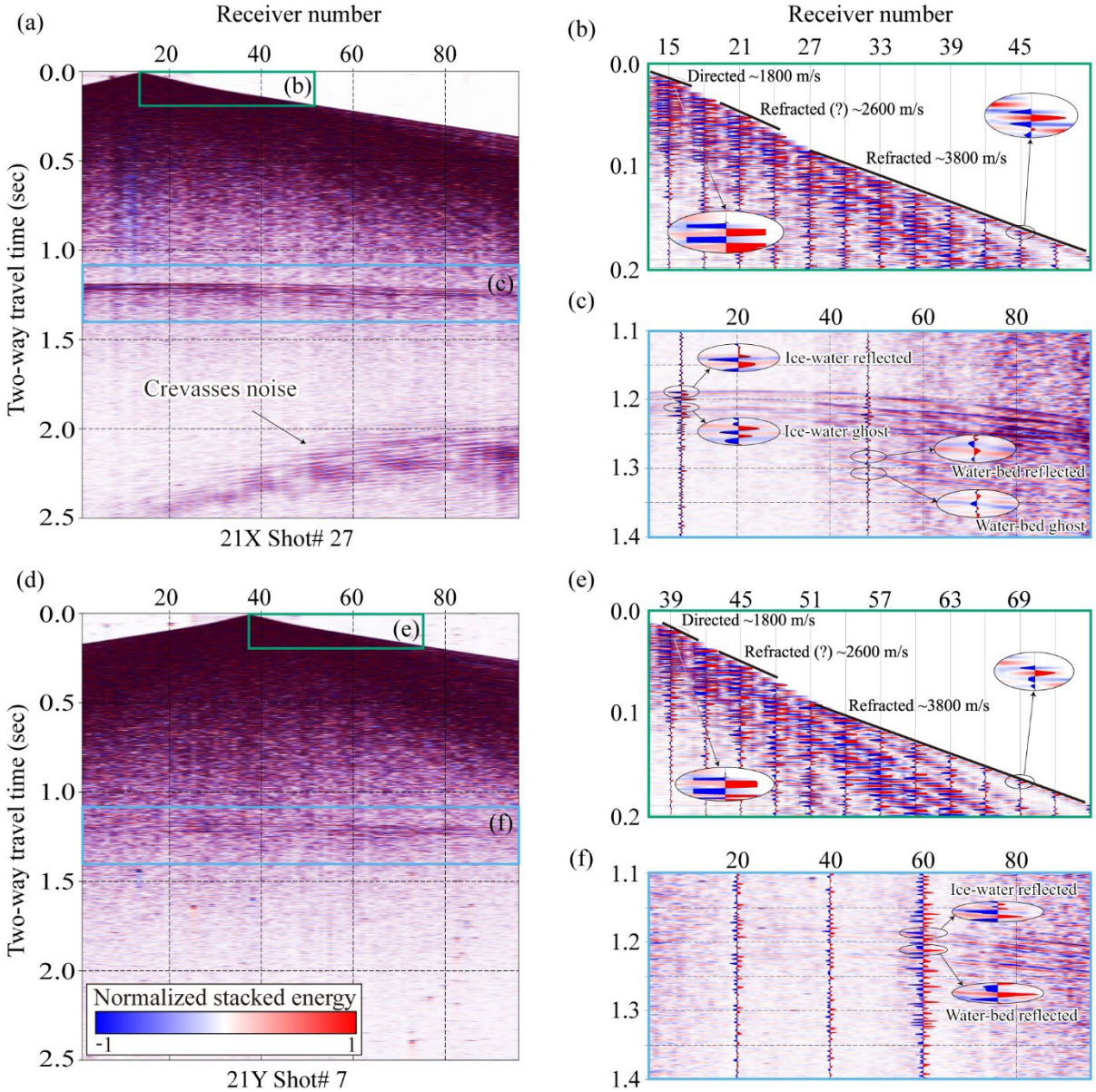

Figure 4: Raw shot records from seismic lines 21X (a) and 21Y (d). Panels (b) and (e) are zoomed-in views of the early arrival window (0.0–0.2 s) from panels (a) and (d), respectively, used to calculate the apparent velocities of the direct and refracted waves. These panels highlight that the first arrivals of both the direct wave (clipped for display) and the refracted wave exhibit positive polarity. The direct wave, propagating through the upper firn layer (0–25 m depth), shows an apparent velocity of approximately 1800 m/s, while the refracted wave traveling through glacier ice has an apparent velocity of about 3800 m/s. Panels (c) and (f) are zoomed-in views of the deeper arrivals (1.1–1.4 s) from panels (a) and (d), respectively. Reflections from the ice–water interface exhibit negative polarity, whereas those from the water–bed interface display positive polarity.

3.2 Figure 6 images are too small as well. Making these subfigures larger would aid interpretation.

➔ We have revised Figure 6 by enlarging each subfigure of the PSTM (Pre-stack Time Migration) sections to enhance the visibility of key reflection signals. The time axis of the sections has been narrowed from the original two-way travel time (TWT) window of 1.0–1.5 seconds to a more focused window of 1.15–1.35 seconds, enabling a clearer visualization of the subglacial lake reflections.

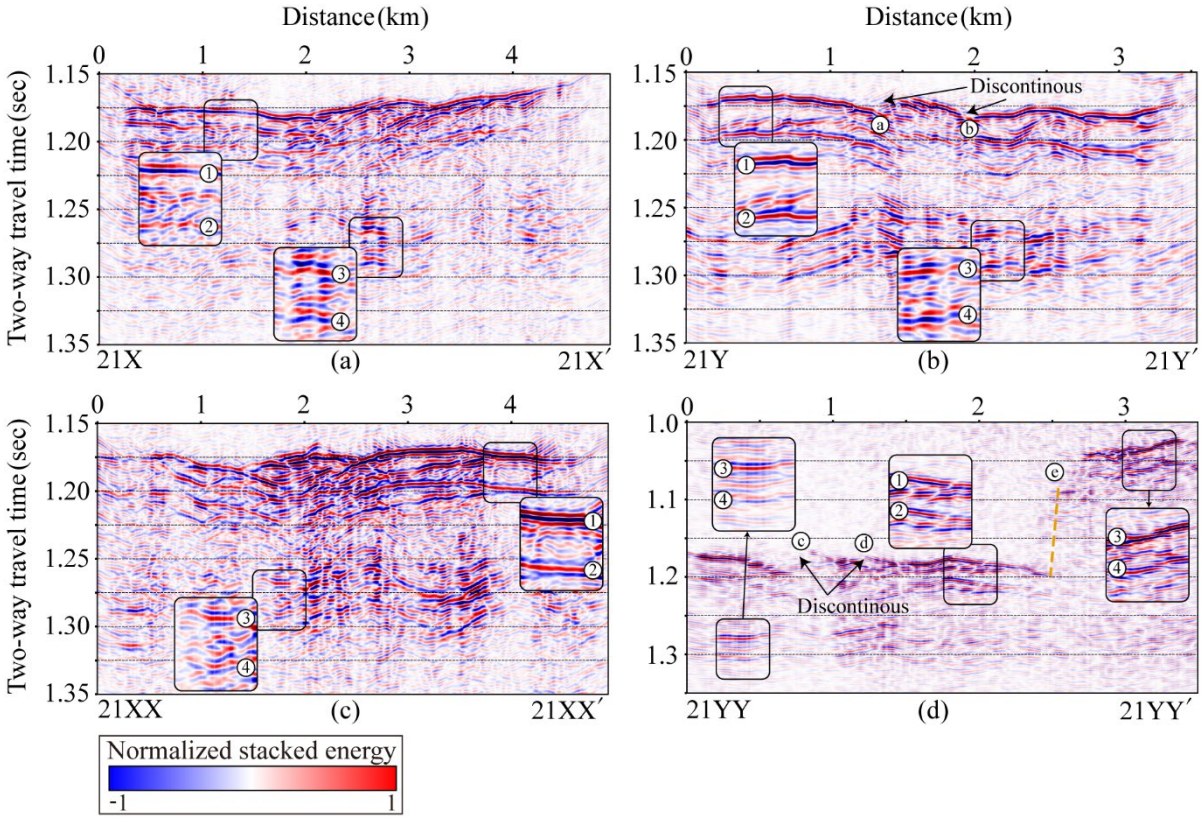

Figure 6: PSTM seismic sections for lines (a) 21X, (b) 21Y, (c) 21XX, and (d) 21YY prior to ghost removal. Ghost reflections appear 25–30 ms beneath the glacier–lake and lake–bed interfaces due to the 25 m source depth.

3.3 Figure 9a looks to have an error. L257 states that this location represents ice over water but the dominant polarity of the basal return is +ve with small –ve side lobes. Also is the wiggle convention of +ve to the right being followed? Currently the right hand wiggle corresponds to the blue (-ve) color coding. This is confusing and should be corrected.

➔ We apologize for the mistake in the previous version of Figure 9, where the polarity was displayed incorrectly during the figure's production. We have revised Figure 9 accordingly. In the updated figure, negative polarity in the wiggle traces is now correctly shown on the left (blue) and positive polarity on the right (red). Additionally, the figure has been enlarged for better visibility, and the previously incorrect time axis labeling has been corrected. For clarity, the term “scour” was revised to “scour-like feature (SLF)” throughout the manuscript and figures.

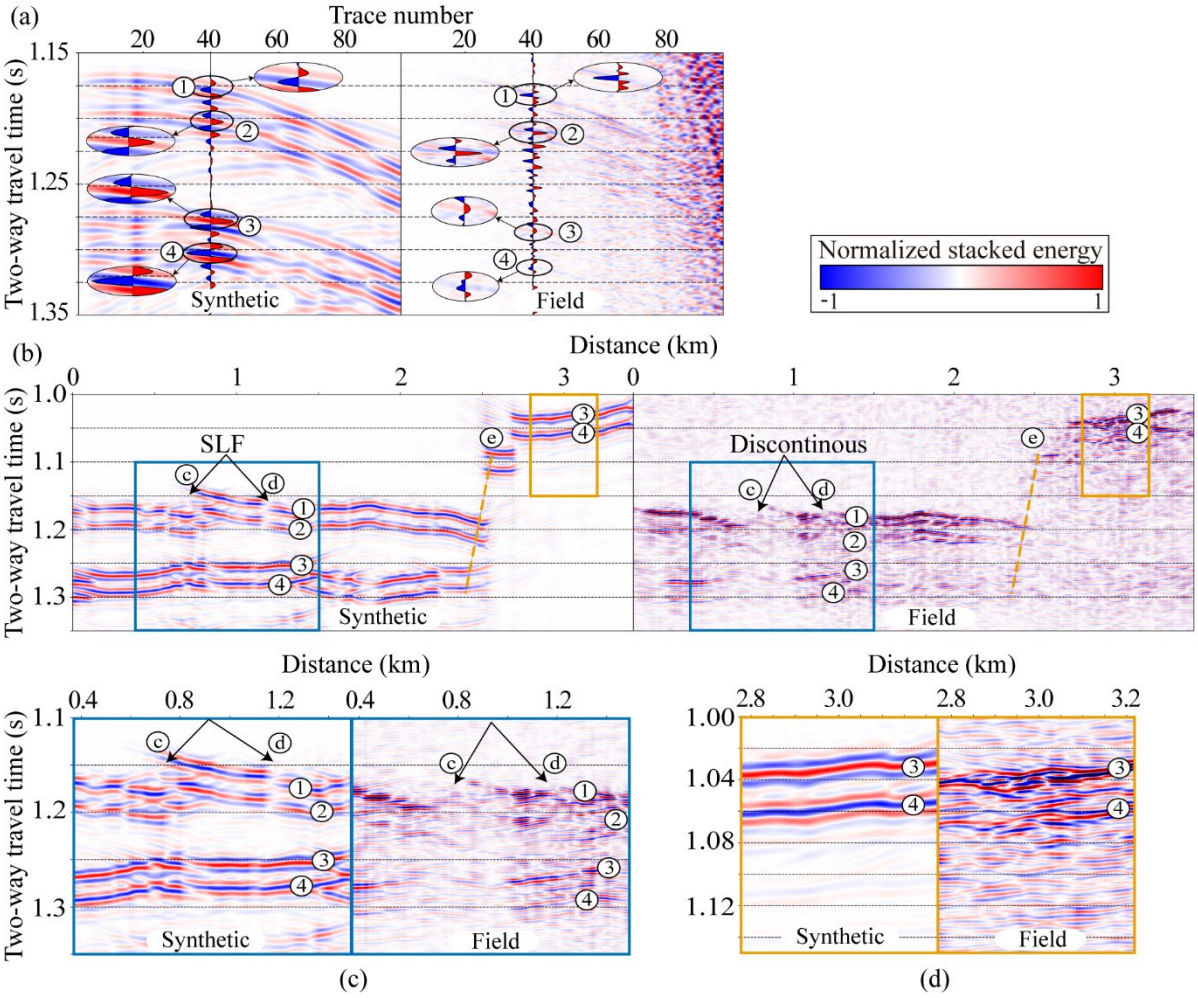

Figure 9: Comparison of synthetic and field seismic data. (a) Shot gather at the same location for synthetic (left) and 21YY field data (right). (b) PSTM comparison between the synthetic model and the 21YY line. (c) Enlarged views of discontinuous reflections (synthetic, field). (d) Comparison of dipping bed reflections (synthetic, field), showing shadow zones and steep basal topography.

Technical corrections

4. The distance annotations shown in figures 2 and 6 should be shown on one of the basemaps.

➔ We revised Figures 1 and 2 to include the locations of SLD2-A, SLD2-B, and SLD2-C. Additionally, to help readers easily understand the orientation of the cross-sectional profiles in Figure 6, we added the X–X' line to Figure 3. Furthermore, the satellite altimetry in Figure 2 has been updated to include the most recent data through July 2024.

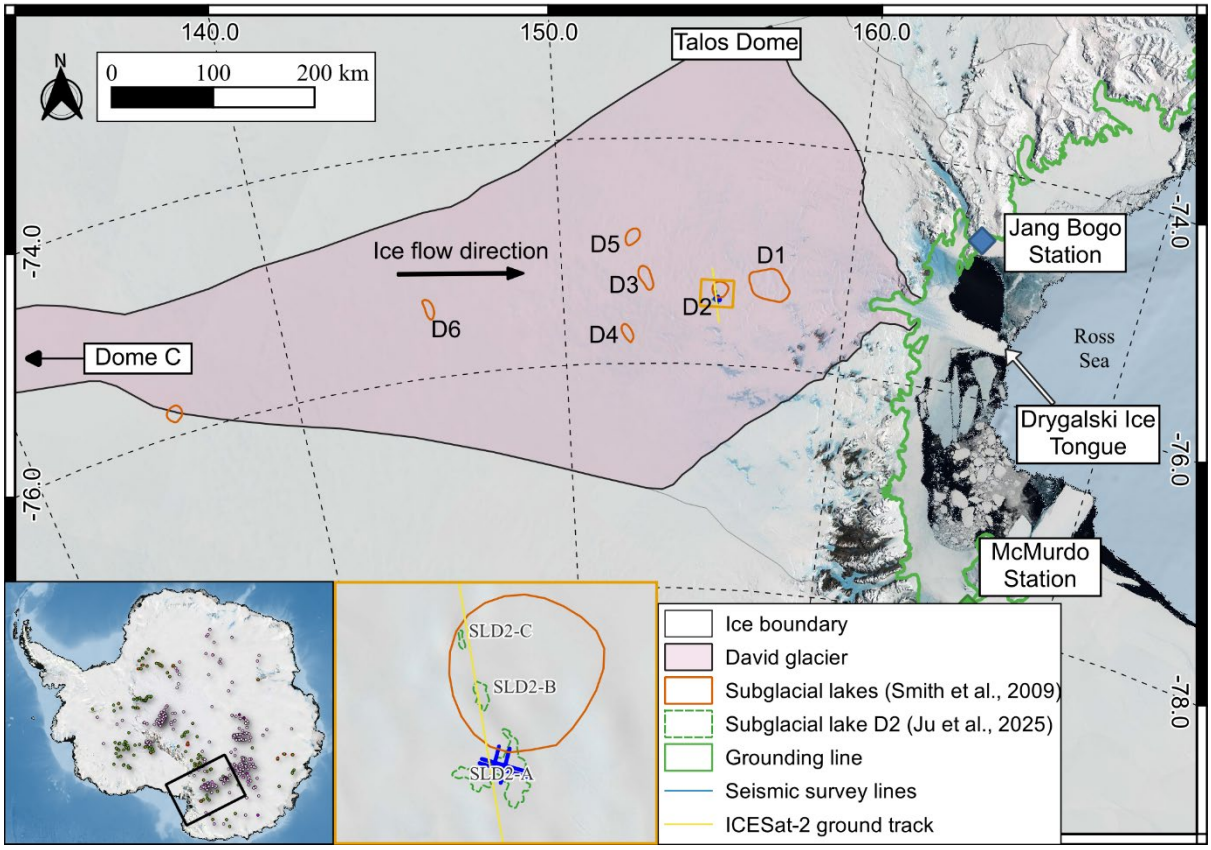

Figure 1: Locations of subglacial lakes D1–D6 in the David Glacier region, Victoria Land, Antarctica (EPSG: 4326–WGS84).

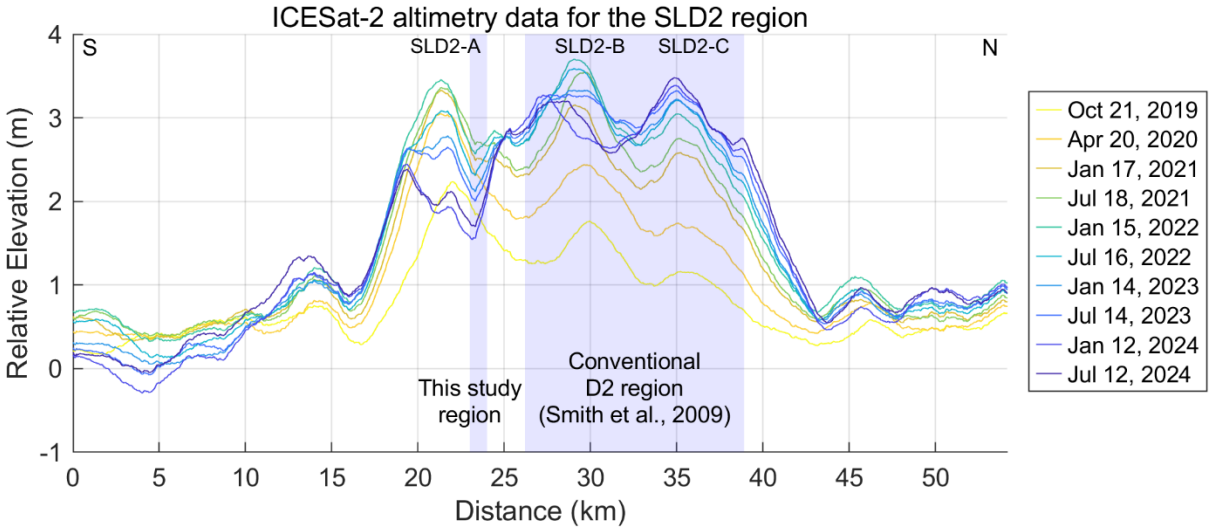

Figure 2: Glacier surface elevation changes derived from ICESat-2 altimetry between 22 April 2019 and 12 July 2024. The X-axis corresponds to the 22 April 2019 dataset, and all subsequent elevation changes are referenced to this date. The light blue shaded region indicates the spatial overlap between the conventional SLD2 region identified by Smith et al. (2009) and our study region.

5. The software used for processing the seismic data should be stated as the naming of routines is not always consistent across processing packages.

➔ We have revised the caption of Figure 5 for clarity. The original mention of "Omega geophysical data processing platform" has been updated to "Omega geophysical data processing platform (SLB)" to specify the software provider.

6. The distinction between active and inactive lakes should be made in the introduction.

➔ We have moved the definitions of stable and active subglacial lakes from Section 2.2 to the Introduction.

(Page 2, Lines 32-39) "Subglacial lakes in Antarctica are generally categorized as either stable or active. Approximately 80% of subglacial lakes in Antarctica are classified as stable subglacial lakes. These closed systems do not exhibit significant surface elevation changes and where subglacial water remains largely isolated, with minimal exchange due to slow and stable recharge and discharge cycles. The remaining 20% are classified as active subglacial lakes, which exhibit surface elevation changes due to episodic water drainage and refilling events (Livingstone et al., 2022). Such active lakes can reduce basal friction as they expand, thereby facilitating glacier flow and, in some cases, accelerating calving processes, ultimately influencing glacier dynamics (Bell et al., 2007; Stearns et al., 2008; Winsborrow et al., 2010)."

7. L79—83 This combination of data used to conclude that the region has contributed to SLR needs more rigour. As this is not the focus of the study I would instead suggest relying on an already published estimate. The ICESat2 surface elevation change results of Smith et al (2020) show the region upstream is thickening over the ICESat2 period.

➔ The relevant section of the manuscript has been revised based on the results and interpretations provided by Smith et al. (2020).

(Page 3, Lines 89-92) "According to Smith et al. (2020), satellite altimetry observations from ICESat-1 and ICESat-2 (20032019) indicate that the grounded portion of David Glacier experienced a mass gain of 3 ± 2 Gt yr^{-1}, whereas the adjacent ice shelves exhibited a mass loss of -1.6 ± 1 Gt yr^{-1}. Although the overall mass balance of David Glacier currently appears stable, it remains uncertain how long this stability can be maintained."

8. L91 'with minimal exchange' I don't know if we know this. To my mind stable lakes just mean water is entering at the same rate it is exiting. More generally I would shift this description of active and stable lakes to the introduction.

➔ Please refer to our response to comment 6, where this issue is addressed in detail.

9. L109-110 repeat L61-63.

➔ We removed duplicate content from lines 109-110.

10. L112 'depressed basal elevations' Really it's the presence of hydropotential sinks as surface topography can dominate subglacial topography.

➔ The paper by Ju et al. (2025), which outlines the D2 subglacial lake area using radar data, has been recently published. We have cited this reference and revised several sentences in the manuscript to incorporate the updated information. Additionally, we have added the hydraulic head map to Figure 3 to provide more context for understanding the subglacial hydrology of the study area.

(Page 5, Lines 113-119) "To better constrain the lake's extent and basal conditions of SLD2, airborne IPR survey data from 2016/17 (Lindzey et al., 2020) and **2018/19 (Ju et al., 2025)** field campaigns indicate that glacier surface elevations in the SLD2 region range from approximately 1820 to 1940 m, with ice thicknesses varying between 1685 and 2293 m. Furthermore, the observations of moderately enhanced radar bed echoes relative to the surrounding area, elevated specularity values (>0.4), depressed basal elevations (≤–350 m), **the presence of a Bain-like topography, a lower hydraulic head than the surroundings,** and low hydraulic gradients (≤ 0.84°) collectively suggest a high potential for the presence of subglacial water beneath SLD2. (**Ju et al., 2025**; Lindzey et al., 2020)."

11. L123 ‘deployed’-> acquired

➔ (Page 6, Line 139) We have changed from
“A total of four seismic lines were **deployed** and designated 21X, 21Y, 21XX, and 21YY” to
“A total of four seismic lines were **acquired** and designated 21X, 21Y, 21XX, and 21YY”.

12. Figure 3. Add hydropotential contours.

➔ Please refer to our response to comment 1, where this issue is addressed in detail.

13. Figure 4. Consider displaying fewer shots and making them larger so polarity can be more easily identified.

➔ Please refer to our response to comment 3.1, where this issue is addressed in detail.

14. L158 ‘A geometry setup was performed...’ -> Acquisition geometry was added to the data...

➔ (Page 10, Line 184) We have revised from
“**A geometry setup was performed** using the raw data and geometry information” to
“**Acquisition geometry was added to the data** using the raw data and geometry information”

15. L159 or soon after – state what software was used for processing.

➔ Please refer to our response to comment 5, where this issue is addressed in detail.

16. Figure 5. Consider showing shot record and zoom before and after processing.

➔ We have added the shot records and PSTM results before and after processing in the Supplementary Information.

17. L181-182. Please state what you are reporting for resolution. (Looks like ¼ wavelength at for ice velocity at the upper end)

➔ We have revised the manuscript to explicitly state that the vertical resolution was calculated based on the quarter-wavelength criterion. The resolution range of 2.01 to 5.27 m was derived using the central frequency of 180 Hz and the range of seismic velocities (1395–3800 m/s) obtained in this study.

(Page 11, Lines 210-212) “Assuming seismic wave velocities between 1395 m/s and 3800 m/s, the corresponding vertical resolutions, **which are calculated using the quarter-wavelength criterion**, range from approximately 2.01 m to 5.27 m. This resolution is adequate for imaging SLD2.”

18. Figure 6. These are too small for me to examine polarity. Please increase in size. You shouldn’t need to reproduce the basemap here if it in presented well previously.

➔ Please refer to our response to comment 3.2, where this issue is addressed in detail.

19. L201 ‘These features may be associated with glacial erosion....’

➔ It is unclear what the question is intended to comment on.

20. L240 ‘P-wave velocity...is faster...’ Strictly speaking it’s an impedance increase.

➔ We have revised the sentence for clarity.

(Page 14, Lines 269-271) “Additionally, on line 21YY, the reflection polarity at the ice–bedrock interface appears as normal polarity, **which indicates an increase in the acoustic impedance**. In other words, this suggests that the P-wave velocity of the bedrock is **higher** than that of the overlying ice.”

21. Figure 9. There are some issues with polarity discussed above. There looks to be a polarity reversal up the step in Fig 9b, which would be compelling and a nice example of how seismic data can show abrupt changes in water at the bed but again it’s hard to see in the field data.

➔ Please refer to our response to comment 3.3, where this issue is addressed in detail.

22. L309-310 ‘hydrological barrier’ hard to say without knowing surface. Again hydropotential contours would be helpful here.

➔ Please refer to our response to comment 1, where this issue is addressed in detail.

23. The conclusion could include statements on the mismatch between the active lake boundary and the area surveyed here and could suggest a location for direct access.

➔ Please refer to our response to comment 1, where this issue is explained in detail. Additionally, we have included a specific recommendation for the potential direct access drilling site in the conclusion section to support future subglacial exploration efforts.

(Page 19, Lines 367-370) “Ultimately, this study identifies the area within a 1 km radius of S 75.422°, W 155.441° as a suitable candidate site for clean hot-water drilling, given its wide spatial extent, minimum estimated water depth exceeding approximately 50 m, and absence of contamination from surface field camps. The site is therefore considered highly appropriate for future exploration of active subglacial lakes.”

Reference:

Ju, H., Kang, S., Han, H., Beem, L. H., Ng, G., Chan, K., Kim, T., Lee, J., Lee, J., Kim, Y., and Pyun, S.: Airborne and Spaceborne Mapping and Analysis of the Subglacial Lake D2 in David Glacier, Terra Nova Bay, Antarctica, J. Geophys. Res.: Earth Surf., 130, https://doi.org/10.1029/2024jf008142, 2025.

Smith, B. E., Fricker, H. A., Gardner, A. S., Medley, B., Nilsson, J., Paolo, F. S., Holschuh, N., Adusumilli, S., Brunt, K., Csatho, B., Harbeck, K., Markus, T., Neumann, T., Siegfried, M. R., and Zwally, H. J.: Pervasive ice sheet mass loss reflects competing ocean and atmosphere processes, Science, 368, 1239–1242, https://doi.org/10.1126/science.aaz5845, 2020.

Supplement of

Seismic data analysis for subglacial lake D2 beneath David Glacier, Antarctica

Hyeontae Ju, Seung-Goo Kang, et al.

Correspondence to: Seung-Goo Kang (ksg9322@kopri.re.kr)

The copyright of individual parts of the supplement might differ from the article license.

S1. Seismic data processed parameters and results

This study utilized the Omega geophysical data processing platform (SLB) for seismic data processing. Among the various processing steps, we provide below the key parameters applied during procedures that directly influence the ice–bedrock interface signal, such as noise attenuation.

1. Anomalous amplitude attenuation (AAA) for the 1st round

AAA is a frequency-domain filtering technique designed to suppress spatially coherent anomalous amplitudes such as swell noise and rig noise, by comparing amplitude spectra across traces and attenuating outliers based on spatial median statistics. The method identifies frequency bands with anomalous energy by comparing each trace's amplitude spectrum within a spatial window to the median of its neighboring traces. Detected anomalies are either scaled or replaced using interpolated values from adjacent traces, preserving relative amplitude relationships. Key parameters include TIME, which defines the temporal window of threshold application; THRESHOLD FACTOR, which sets the amplitude level considered anomalous; and SPATIAL MEDIAN WIDTH, which specifies the number of adjacent traces used for median computation. Proper tuning of these parameters is essential to avoid signal distortion while effectively attenuating coherent noise. AAA is particularly useful in prestack data conditioning as it enhances seismic data quality without compromising true subsurface reflections (SLB, 2025a).

- SPATIAL MEDIAN WIDTH: 21 traces
- Threshold factor tables:

TIME	THRESHOLD FACTOR
0	15
1000	10
3000	7
4000	6

2. Curvelet transform-based filter for 1st round (Figure S43b)

Curvelet Transform is a multi-scale, multi-directional decomposition technique that provides a sparse representation of seismic data by capturing curved wavefronts more efficiently than conventional fourier or wavelet transforms. An important aspect of the Curvelet Transform implementation involves user-defined control over the scale and angle bounds that determine which components of the data will be transformed. The LOWER BOUND OF SCALE and HIGHER BOUND OF SCALE specify the range of spatial frequencies (scales) to be included in the transform. Lower scales correspond to coarse, low-frequency components, while higher scales capture fine, high-frequency structural details. The LOWER BOUND OF ANGLE and

HIGHER BOUND OF ANGLE define the directional sectors (angles) within each scale to be analyzed. This allows selective enhancement or suppression of events based on their dip or propagation direction (SLB, 2025b). Figure S1 illustrates how the f–k domain is partitioned into curvelet panels by scale and angle. Adjusting these bounds allows for targeted signal processing, such as isolating curved events or attenuating directionally coherent noise. These parameters provide valuable flexibility in customizing the transform for specific seismic applications.

- Panel manager

LOWER BOUND OF THE SCALE	HIGHER BOUND OF THE SCALE	LOWER BOUND OF THE ANGLE	HIGHER BOUND OF THE ANGLE
2	2	1	3
2	2	8	10
3	3	1	6
3	3	13	18
4	4	1	6
4	4	13	18

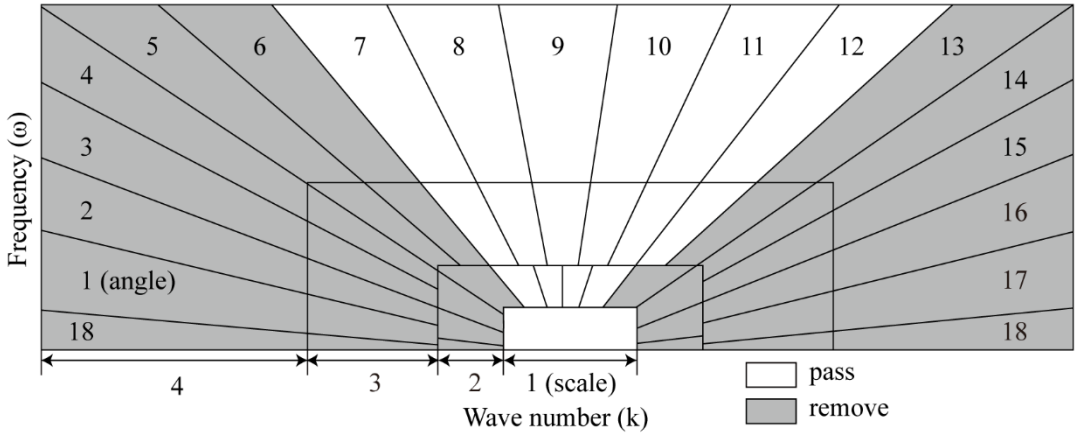

Figure S1: Illustration of the panel manager. In the f-k domain, the hatched area is identified as noise and removed accordingly.

3. Surface-consistent deconvolution

Surface-Consistent Deconvolution is a technique for generating and applying deconvolution operators that are consistent across seismic sources, receivers, offset ranges, and CMP locations (SLB, 2025c; Yilmaz, 2001).

Key processing parameters used in this workflow include:

- CONSTANT_ACOR_LENGTH = 100: Defines the half-length of the autocorrelation window used in operator design, balancing spectral resolution and filter stability.

- WHITE NOISE PERCENT = 0.01: Adds 1% white noise to stabilize the autocorrelation estimation and prevent over-whitening of the signal.
- PREDICTION DISTANCE = 2.5: Specifies the prediction lag in the predictive filter design; this parameter controls the temporal range of the filter's effect, influencing multiple suppression and resolution.

4. Anomalous amplitude attenuation (AAA) for the 2nd round
   - Spatial median width: 11 traces
   - Threshold factor tables:

Time	Threshold factor
0	8
1000	6
3000	4
4000	3

5. Curvelet transform-based filter for the 1st round: same as 1st round parameter

6. Frequency-offset coherent noise suppression (Figure S3.c)

The frequency–offset (F-X) Coherent Noise Suppression (FXCNS) module is designed to attenuate near-surface shot-generated coherent noise, such as dispersive surface waves and trapped modes, which interfere with primary seismic reflections, particularly in 3D shot or receiver gathers with irregular spatial sampling (Hildebrand, 1982). FXCNS operates in the frequency domain by modeling coherent noise using fan filters and estimating it in a least-squares sense for each trace based on local neighbors within a specified azimuthal sector. The estimated coherent noise is then subtracted from the original signal, preserving true reflection events (SLB, 2025d).

- LOW PASS VELOCITY: 100
- LOW STOP VELOCITY: 300
- HIGH PASS VELOCITY: 8000
- HIGH STOP VELOCITY: 10000

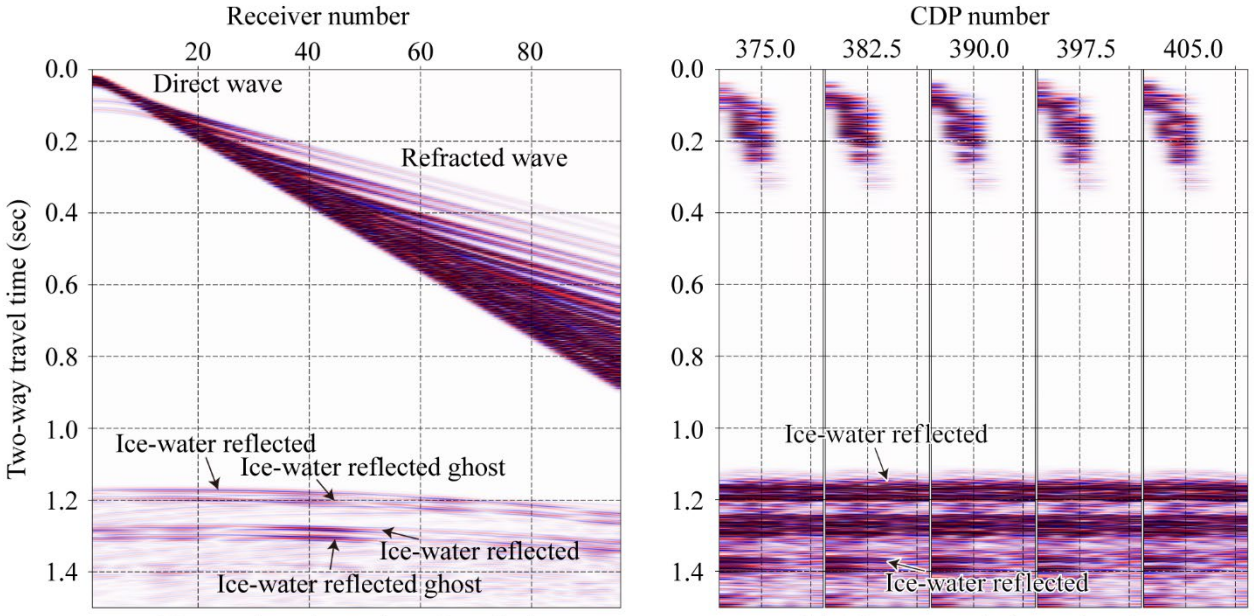

(a) Raw data shot gather of synthetic (b) After pre-stack time migration

Figure S2: Results before and after data processing. (a) Synthetic raw data of shot gather #1. (b) Result after pre-stack time migration.

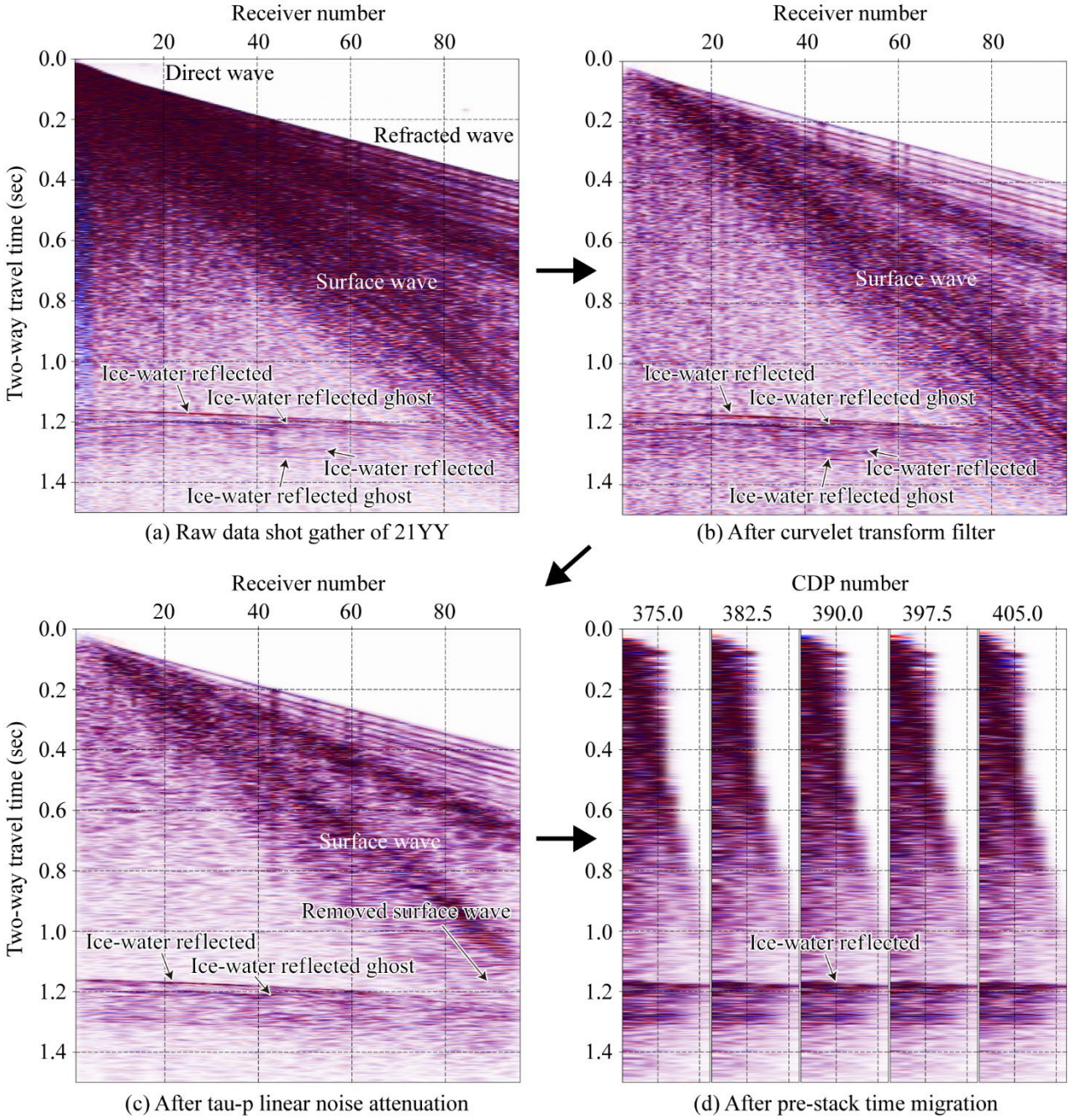

Figure S3: Results at each stage of data processing. (a) Shot gather #1 from 21YY. (b) Removal of high-frequency random noise and coherent linear noise. (c) Application of a frequency-offset coherent noise filter and tau-p linear noise attenuation for surface wave removal. (d) Result after applying pre-stack time migration.

References

Hildebrand, S. T.: Two representations of the fan filter, Geophysics, 47, 957–959, https://doi.org/10.1190/1.1441363, 1982.

SLB: *Omega Geophysical Processing System – Anomalous Amplitude Noise Attenuation (ANOMALOUS_AMP_ATTEN) Module Documentation*, Version 27.14, SLB manual, Houston, TX, 2025a.

SLB: *Omega Geophysical Processing System – Curvelet Transform (CURVELET_TRANSFORM) Module Documentation*, Version 22.1, SLB manual, Houston, TX, 2025b.

SLB: *Omega Geophysical Processing System – Surface-Consistent Deconvolution Analysis (SC_DCN_SPCTRL_ANL) Module Documentation*, Version 13.18, SLB manual, Houston, TX, 2025c.

SLB: *Omega Geophysical Processing System – F-X Coherent Noise Suppression (FXCNS) Module Documentation*, Version 3.16, SLB manual, Houston, TX, 2025d.

Yilmaz, Ö.: Seismic data analysis: Processing, Inversion, and Interpretation of Seismic Data, Appendix B.8 (Surface-Consistent Deconvolution), Society of Exploration Geophysicists, 262–266 pp., 2001.